Hydrol. Earth Syst. Sci. Discuss., 9, 11267–11318, 2012
www.hydrol-earth-syst-sci-discuss.net/9/11267/2012/
doi:10.5194/hessd-9-11267-2012

Hydrology and Earth System Sciences Discussions

Floods and wetlands: combining a water-balance model and remote-sensing techniques to characterize hydrological processes of ecological importance in the Tana River Delta (Kenya)

C. Leauthaud[1,2], S. Duvail[2,3], G. Belaud[4], R. Moussa[5], O. Grünberger[1], and J. Albergel[1]

[1]IRD, UMR LISAH, 2 Place Viala, 34060 Montpellier, France
[2]Kenya Wetland Biodiversity Research Team (KENWEB), Kenya
[3]IRD, UMR 208 Patrimoines Locaux (PALOC), France
[4]Supagro, UMR G-eau, 34060 Montpellier, France
[5]INRA, UMR LISAH, 2 Place Viala, 34060 Montpellier, France

Received: 12 September 2012 – Accepted: 18 September 2012 – Published: 4 October 2012

Correspondence to: G. Belaud (belaud@supagro.inra.fr)

Published by Copernicus Publications on behalf of the European Geosciences Union.

Abstract

The Tana River Delta (TRD) provides a multitude of ecosystem services for the local communities including fishing, farming and livestock keeping. The hydrological regime of its river determines for a large part the environmental health of the delta. The development of upstream irrigation schemes and hydroelectric infrastructure can seriously impact the ecological status of the TRD. The Tana Inundation Model (TIM) presented here is the first known hydrological model of the TRD. Using it, we quantify essential hydrological variables of ecological importance for 2002–2011 such as flood extent and duration, flood timing and frequency, flood peaks and water height. TIM also provides an annual water balance. The model simulates river inflows and outflows, precipitation, overland flow, evapotranspiration and infiltration. The TRD is characterized by scarce hydrological data and a high cloud cover limiting the use of many remote sensing techniques. The methodology therefore combined a conventional water-balance analysis with the extraction of inundation extents from MODIS satellite imagery at a medium spatial and temporal resolution. In non extreme years and for the actual configuration of the Tana River, the flooded area exceeds 560 km^2. Floods over 200 km^2 occur approximately every two years, with a mean duration of less than 25 days. River discharge from the upper catchment counts for over 96 % of the total water inflow. This study provides the first known estimates of these variables for the Tana River Delta and is therefore primordial for the management of the water and other natural resources of the zone. The hydrological model based on the Generalized Likelihood Uncertainty Estimation (GLUE) is generic enough to be applied to other catchments with scarce hydrological data.

1 Introduction

Wetlands are amongst the most threatened ecosystems worldwide (Vitousek et al., 1997). With rivers, their global coverage of the Earth's surface is over 4 % (Prigent

HESSD
9, 11267–11318, 2012

et al., 2001). It is rapidly declining with an estimated overall loss in the global average maximum inundated area of 6 % from 1993 to 2007 (Prigent et al., 2012). As a strategic global resource, these systems need to be preserved and restored (Tockner and Stanford, 2002). Indeed, wetlands are increasingly recognized as ecosystems essential to human activities (Mitsch and Gosselink, 2000) as they provide a wide range of ecosystem services (Daily, 1997; Millennium Ecosystem Assessment, 2005), including food supply, basic material provisioning, water supply and purification, ground-water recharge, climate regulation, coastal protection, carbon sequestration, biodiversity conservation and tourism. The hydrological processes of the adjacent river (Mitsch and Gosselink, 2000), in particular, flood extent, timing, frequency, duration, flood peaks and water height, largely determine the physical, chemical and biological properties of wetlands. Modifications in up-stream land use, development projects such as hydropower dams, and increased water withdrawal, in conjunction with climate change, are strongly impacting downstream wetlands and their users. For example, the inundated area of the Hadejia-Jama'are floodplain in Nigeria decreased since the 1960s and 1970s by 60 to 76 % as a result of hydrological changes (Barbier and Thompson, 1998) and 88 % of the seasonal wetlands with low moisture of the Choke Mountain Range, in Ethiopia, were converted to cultivated land between 1986 and 2005 (Teferi et al., 2010). Dam construction has altered other large wetlands throughout Africa: the Senegal River Delta wetlands in Mauritania (Duvail and Hamerlynck, 2003) and in Senegal (Lamagat et al., 1996; Bader et al., 2003), the Inner Delta of the Niger River in Mali, the Waza Logone in Cameroon (Loth, 2004), the Medjerda River in North Africa (Zahar et al., 2008), the Tana River in Kenya (Maingi and Marsh, 2002); and others are threatened such as the Okavango Delta in Botswana (Milzow et al., 2009), the Rufiji Delta (Duvail and Hamerlynck, 2007) and the Omo River Delta in Kenya and Ethiopia. The link between the inundation dynamics and the health of the adjacent ecosystems is often mentioned (Zeilhofer and Schessl, 2000; Toogood et al., 2008; Merritt et al., 2010). Many studies have focused on quantifying the processes involved, describing their dynamics and establishing relationships with the riparian ecosystems' status (for

HESSD
9, 11267–11318, 2012

a literature review, see Merritt et al., 2010 and Poff and Zimmerman, 2010). However, as relationships between flow alteration and ecological responses are often dependent on the type of alteration, ecosystem and location, no general and rapidly transferable relations exist (Poff and Zimmerman, 2010). Our objectives were to: (1) construct a parsimonious hydrological model using satellite imagery, (2) quantify the major hydrological processes that occur in the Tana River Delta (TRD) and (3) establish a relationship between the inundation extent and the hydrograph of the Tana River. More specifically, we describe the inundation extent, timing, frequency, duration, flood peaks and water height in the TRD as a function of river discharge 250 km upstream. A yearly water balance as well as a description of the major hydrological processes, along with the uncertainties relative to the calibration procedure, are also provided. The Tana Inundation Model (TIM) was constructed as a tool to analyse the possible past and future impacts of upstream dams on the inundation characteristics of the TRD. It can be used to model short to medium term trends in ecological responses to changing hydrological conditions. Finally, by presenting an inundation model based on remote sensing images and the Generalized Likelihood Uncertainty Estimation (GLUE) (Beven and Binley, 1992) and applied to the TRD, this paper contributes to the growing literature on the use of hydrological modeling for prediction in ungauged basins (Sivapalan et al., 2003).

2 Hydrological modeling and the use of remote sensing techniques in poorly gauged basins

2.1 Hydrological modeling: concepts and approaches

Important environmental questions need to be addressed that require hydrological data. Yet, a vast majority of catchments worldwide lack long-term and reliable hydrological and climatic data. With the further disappearance of measuring stations in the last 30 yr (Fekete and Vörösmarty, 2007), hydrologists need to find new ways to calibrate and validate their models. In the last decades, many satellites have been launched

HESSD
9, 11267–11318, 2012

to monitor environmental variables. This gives a new perspective for researchers who can then integrate remotely sensed spatial information into the modeling procedures. However, there are no standard methods to do so as the choice of the model and remote sensing (RS) data depends on the objectives of the study, the spatial extent of the studied zone, the available hydrological, topographic, soil and climatic data and on the climatic conditions (such as cloud cover). In some well studied basins, several models using different RS techniques have been developed (such as the Okavango Delta, Botswana: Bauer et al., 2006; Hughes et al., 2006; Wolski et al., 2006; Milzow et al., 2009, 2011), but models are still nonexistent for most basins. Many hydrological models and concepts have been applied to wetlands, going from conceptual models, through lumped, semi-distributed to distributed models. The approaches used differ in their physical basis, complexity and data requirements and the choice to use a specific one depends on the objectives of the study. Although conceptual lumped models lack specific spatial representation, they are usually less data-demanding and require few and (often) easily identifiable parameters. These kind of models have been applied to many wetlands worldwide such as the Okavango Delta in Botswana (Wolski et al., 2006) or the Inner Delta of the Niger River in Mali (Mahe et al., 2011). Despite their simplicity, they are useful to determine important hydrological processes and are easy to transfer to decision makers for management purposes. The TRD in Kenya, with its large wetlands, upstream dams and scarce data constitutes an ideal ground to test our ability to provide information through hydrological models and RS techniques in a poorly gauged basin. For the above reasons, a water-balance model is used in this study, where water storage is modeled using a unique reservoir. The model is calibrated using the GLUE methodology with remote-sensing data and field data.

HESSD
9, 11267–11318, 2012

2.2 The role of remote sensing in hydrological modeling of flood extents

2.2.1 Choice of satellite imagery

The use of remote sensing data facilitates the study of water bodies in remote and difficult to access areas. In recent years, different remote sensing techniques have been used to detect water bodies and their characteristics (water extent, height, variability, vegetation cover, sediment load, etc.). Synthetic Aperture Radar imagery is very popular because of its high spatial resolution and its capacity of mapping water under thick vegetation. However, the radar signals change continuously due to wind induced-waves, especially in the C-band, limiting the use of this band for water detection (Alsdorf et al., 2007). L-band data are limited by their low orbital repeat cycles, cost and limited archives. Passive microwave data have been used to detect flooded surfaces (Sippel et al., 1998; Ticehurst et al., 2009), but are limited by low spatial resolution. Thermal satellite data have been used to map inundated areas (Leblanc et al., 2011) but to our knowledge at an inadequate monthly time-scale to characterize rapidly changing inundation extents. An alternative solution is the use of passive optical/infrared sensors on board the Landsat, Moderate-Resolution Imagery Spectroradiometer (MODIS) and SPOT satellites.

The MODIS instruments on-board the Terra and Aqua satellites have been providing daily data for 36 spectral bands between 0.405 and 14.385 µm at a 250 m to 1 km resolution since 2000 and 2002, respectively. They have been used to successfully map flooded areas, inundation patterns, water levels (Ordoyne and Friedl, 2008), seasonality of lake systems (Feng et al., 2012), the extent of annual flooding (Sakamoto et al., 2007), wetland mapping and inundation maps (Ticehurst et al., 2009; Islam et al., 2010). Despite the moderate resolution, their long-term data and frequent overpass make them a good tool to monitor large to medium size wetland complexes. Like other optical sensors, MODIS images are subject to cloud cover, limiting their use during periods with cloudy skies. However, certain level-3 products provide high-quality aggregate images such as the MYD09A1 product. The latter is a 500-m resolution image where

HESSD
9, 11267–11318, 2012

each pixel contains the best possible observation during an 8-day period, corrected for atmospheric gases and aerosols. Two bands also describe the quality of each pixel and the state of the surface reflectance data regarding aerosols, presence of clouds or cloud shadow and other variables, so that masking poor quality pixels is possible. In regard of the advantages cited here, and of their rapid and free-of-cost availability, we decided to use the MODIS MYD09A1 product to obtain a time-series of inundation maps in the TRD.

2.2.2 Choice of index

Differences in the spectral signature of land and water covers are used to distinguish water bodies from other surfaces. Many Water Indices have been developed using different spectral bands and different satellite data (Gao, 1996; McFeeters, 1996; Rogers and Kearney, 2004; Xu, 2006). However, they don't always distinguish between flooded and non-flooded vegetation. A major characteristic of the TRD is the frequent presence of a dense and low flooded vegetation covering the water. Oliesak (2008) used the Modified Normalized Difference Water Index (Xu, 2006) to map the open water bodies in the Inner Niger Delta and the Normalized Difference Water Index of Gao ($NDWI_{Gao}$) (Gao, 1996) to include the vegetated water. Despite large differences in spatial extent between the Inner Niger Delta and the TRD, some main characteristics of the wetlands (flooded vegetation of *Echinochloa stagnina* (Retz) P. Beauv) are identical. Following this approach, the $NDWI_{Gao,M2–5}$ index (MODIS spectral bands two and five) was selected to determine inundation extent.

3 The Tana River Delta, Kenya: a wetland, scarce data and important questions

3.1 Context: the socio-economic and environmental situation

With a total surface of over 95 000 km^2 (International Livestock Research Institute, 2012), the Tana River catchment (Fig. 1) is one of the largest in Kenya. The Tana

HESSD
9, 11267–11318, 2012

River Delta itself is an area of approximately 1300 km^2 and roughly extends between the main towns of Garsen, Malindi and Lamu. It is home to over 100 000 inhabitants (Kenya Population Census, 2009), essentially from the Pokomo, Orma, Somali, Wardei and Wata communities. The delta provides a whole range of natural resources for the local communities who mainly rely on agricultural production, fishing and livestock keeping (Leauthaud, 2009; Duvail et al., 2012; Leauthaud et al., 2012) for subsistence. Despite the high productive potential of the wetlands, the region is among the poorest in Kenya and its 2009 indicators of human well-being (United Nations Development Programme, 2010) are extremely low. To aggravate the situation, in recent years, many biofuel and large irrigation schemes have been initiated in the zone, which will deprive the local communities of essential land and water resources (Duvail et al., 2012). Alongside the economical and human value of the TRD, its complex landscape mosaic has an exceptional biodiversity value (Hamerlynck et al., 2012).

3.2 The Tana River in its lower catchment

The Tana is the largest river in Kenya, and flows over nearly 1000 km from Mount Kenya and the Aberdare Mountains to the Indian Ocean. Its flowing pattern is bi-modal, with peak flows during the long and short rainy seasons. The mid and lower catchment of the Tana River are semi-arid and essentially used for livestock keeping, except along the river borders where subsistence farming is practiced. In this semi-arid environment, the Tana River (Fig. 1) is the main water resource for its inhabitants (Emerton, 2003; Terer et al., 2004; Leauthaud et al., 2012). It is also used for hydroelectric production. Over the past fifty years, five major reservoirs (Fig. 1) have been built in the upper basin which have significantly modified the hydrological regime of the river, with a 20 % decrease of the peak flow in May (Maingi and Marsh, 2002). Other projects, in particular those of the Grand Falls Dam, could have greater impacts on the flooding processes downstream in a near future.

HESSD
9, 11267–11318, 2012

Although the river between Garissa and Garsen drains nearly 42 000 km^2 (International Livestock Research Institute, 2012), only temporary rivers flow into it within this stretch such as Laga Tula, the Laga Galole and the Laga Tiva. Maingi and Marsh (2002) consider that flood propagation and losses due to evaporation are the major hydrological processes that occur within this stretch. Indeed, floodplains spread out all along the river and can cause significant evaporation and water loss due to overflow. However, recent studies for the construction of the Grand Falls Dam suggest that the temporary rivers could convey important amounts of water. Water abstraction at the Bura irrigation scheme and the 16 800 ha (Duvail et al., 2012) Tana Delta Irrigation Project (TDIP) could also modify river discharge. However, with a hypothetical water requirement of 2 l s^{-1} ha^{-1} and a cultivated surface of 4000 ha, they would not alter significantly to Tana River discharge during peak flows.

3.3 Climate and pedological characteristics

Precipitation is highly variable throughout the mid and lower catchment. It increases from 373 ± 202 mm (mean and standard deviation) in Garissa (1962–2008, data from the Kenya Meteorological Department, Kenya. Years with over one month missing data were excluded) to 530 ± 202 mm in Garsen (1972–1986) then to 1098 ± 306 mm in Malindi (1962–2008) (Fig. 1). The rainfall pattern is bi-modal, with two rainy seasons extending from April to June and from November to December which correspond to the inundation periods for the Tana River in natural conditions. The relative timing of the precipitation in the TRD and the flooding events is very variable, but precipitation would usually occur before the flood events. To our knowledge, precipitation does not induce the floods itself but would rather acts as a "wetting" event before the arrival of the flood wave. This is significant for the local ecosystems as it initiates growth before the arrival of the floods. Surface runoff from outside the floodplains is probably limited, except in high rainfall years, when the temporary rivers draining the surrounding terraces are activated. Mean temperature in the delta (1998–2009, from the Tana Delta Irrigation

HESSD
9, 11267–11318, 2012

Project measurements, TDIP, 2°316′22.07″ S, 40°11′00.55″ E) is of 28 °C, with a mean maximum and minimum of respectively 31 °C in March and 26 °C in July.

The soils of the Tana River Delta are developed on recent alluvial deposits from the river. The main soil types encountered are deep, well drained, dark brown and cracking vertisols and fluvisols (Kenya Soil Survey,1984a, b). Here and there, small island-like shaped sand dunes form slightly higher grounds where woodlands and forests are established. The interaction between surface water and groundwater remains unclear. The clayey nature of the TRD soils probably limits the infiltration of water in the floodplains during inundation events once the soil is swollen and the cracks reduced. However, the inundations still recharge the groundwater, as testified by the village wells that fill up or empty according to the inundation events. Compared to the water brought by the Tana River, regional groundwater flows to the delta are probably insignificant due to low precipitation in the surrounding semi-arid zones and to a low regional topographic gradient.

4 Hydrological and remote sensing data for the Tana River Delta

4.1 Pre-analysis of the available hydrological data

To monitor the Tana River, three gauging stations were historically available in the Lower Tana and maintained by the Water Resource Management Authority (WRMA), located respectively at Garissa (0°27′49.19″ S, 39°38′11.77″ E), Hola (1°30′00.00″ S, 40°02′00.17″ E) and Garsen (2°16′09.36″ S, 40°07′16.32″ E) (Fig. 1). Of the studied portion of the Tana River, the gauging station of Garissa (code: RGS 4G01), approximately 250 km upstream of the TRD, is the only remaining long-term station (1941–current). As its chronic was incomplete, missing data were completed for the Tana Inundation Model (TIM) by linear interpolation, except for two periods coinciding with a flood event (5 May 2003–31 October 2003 and 31 March 2005–4 August 2005) for which this method is inappropriate. The historical discharge records at Hola (1949–1988)

HESSD
9, 11267–11318, 2012

and Garsen (1951–1998, code: RGS 4G02) are extremely lacunary. As the data from the Hola station prior to 1972 presented an abnormal increase through time possibly explained by a change in the rating curve for this station, the Hola discharge data were excluded from the study. There seemed to be no anomalous tendency in the Garissa and Garsen time-series. In 2010, WRMA, in conjunction with our research project, re-installed a stage board at the Idshowe bridge near Garsen (2°17′19.30″ S, 40°07′35.74″ E) and a rating curve is under construction.

The original discharge datasets used in this study were obtained from WRMA in Nairobi and Garissa. Maximum peak discharges in Garissa were 1622 $m^3 s^{-1}$ in 1941 then 1585 $m^3 s^{-1}$ in 1961. Floods are largely attenuated and smoothed out between the two stations (Fig. 2), with a loss in total transiting volume (Table 1) probably due to strong evaporation within the floodplains. To calculate water gain or loss between the two stations and the mean total volume of water flow, the year was divided into two hydrological seasons starting from 1 March and the 1 September which correspond to the mid-dry seasons and therefore to the low water seasons. To avoid erroneous results, seasons with more than 20 % of missing data were excluded (10 seasons for Garissa for 1941–2009; 60 for Garsen for 1951–1998). The remaining missing data, respectively 2.3 % (542 days) and 6.0 % (397 days) for Garissa and Garsen (for the previously mentioned dates), were filled in by linear interpolation. Mean volume ratio of water transiting from Garissa to Garsen was of 0.76 ± 0.28 for the available floods (Table 1): the volume of transiting water decreases from Garissa to Garsen. These preliminary results support the idea that the major processes to take into account to reconstruct the recent discharge data at the TRD inlet are the flood propagation within the main channel then the overflowing into the floodplains and consequent loss of water between Garissa and Garsen.

HESSD
9, 11267–11318, 2012

4.2 Reconstitution of the river discharge at the TRD input through a non-linear routing model

Discharge measurements at the delta inlet were reconstituted using a flood routing model (Lamagat et al., 1993). The latter is adapted to large rivers with overflow and has been applied to many African rivers including the Niger and Gambia Rivers (Lamagat et al., 1993; Belaud et al., 2010). The approach relies on a theoretical analysis of the diffusive wave equation (Lamagat et al., 1993) and takes into account varying propagation trends in low and high flow regimes. It establishes two empirical relationships from a calibration period between the water-levels or discharges at two stations (Q_1 and Q_2) and between the upstream station and a delay time T. The method is particularly efficient when a large number of floods are available for calibration (Belaud et al., 2010). To do so, the upstream and downstream hydrographs are divided into N elementary intervals then a linear regression is carried out between the two stations for different delay times T and for each interval. The delay time that minimizes the quadratic error function defined as RMSE = $\sqrt{\sum_k \frac{1}{n}(Q^{o}_{2,k} - Q^{s}_{2,k})^2}$ is chosen (where n is the number of observations per interval and Q^{o} and Q^{s} are the observed and simulated water level or discharge at the second station), thus maximizing the correlation between Q_1 and Q_2. In this study, a 10-day moving average of the Garissa discharge was used as the input for the flood propagation model. The number of intervals N was set to the typical value of 20 (Belaud et al., 2010). Calibration was undertaken with observations from 01 December 1986 to 29 June 1991. A back-and-forth method was used to manually correct and smooth out the obtained functions for them to have a monotonous behavior. The daily discharge was then obtained by calculating the daily average discharge from all the simulated points. Validation was carried out on the remaining data by visual comparison of the observed and simulated hydrographs at Garsen and through the calculation of the Nash-Sutcliffe coefficient (NS), the Absolute Mean Error (AME) and the Mean Absolute Error (MAE) as defined by Dawson Dawson et al. (2007) (Table 4) for the available observed and simulated data from 1963 to 1998.

HESSD
9, 11267–11318, 2012

The discharge at Garsen (Q_2) and time delay (T), obtained through the non-linear propagation model, are defined in the Eqs. (1) and (2), where Q_1 is the discharge at Garissa:

$$\begin{aligned} &Q_1 \in [0,320], \\ &\quad Q_2(t) = -0.0014 \cdot Q_1^2(t-T) + 0.9557 \cdot Q_1(t-T) \\ &Q_1 > 320, \\ &\quad Q_2(t) = 0.04692 \cdot Q_1(t-T) + 145.69 \end{aligned} \tag{1}$$

$$\begin{aligned} &Q_1 \in [0,36], \\ &\quad T = 5 \\ &Q_1 \in [36,78], \\ &\quad T = 0.0033 \cdot Q_1^2 - 0.3715 \cdot Q_1 + 14.256 \\ &Q_1 > 78, \\ &\quad T = 3.5588 \cdot \ln(Q_1) - 10.085 \end{aligned} \tag{2}$$

The resulting curves are typical of an overflowing river with a very low slope. Downstream discharge increases with the upstream discharge and the water line has a slope different from the river floor. At high discharges, the rate of change decreases due to overflowing into the floodplains and the consequent evapotranspiration. The time-delay first decreases then increases as the water overflows into the large floodplains. According to the model, a flood of 500 $m^3 s^{-1}$ will take approximately 12 days from Garissa to reach Garsen. For the calibration period, NS was 0.89, AME of 74 $m^3 s^{-1}$ and MAE of 10 $m^3 s^{-1}$. The latter were respectively of 0.87, 107 $m^3 s^{-1}$ and 12 $m^3 s^{-1}$ for the whole validation period. The model reproduces in a satisfactory manner the observed discharges at the Garsen station. According to the model, the flood propagation processes from Garissa to Garsen seem to have remained identical throughout the 1963–2011 period even though dams were constructed during this time in the upper part of the river. The dams therefore would have modified the volume of transiting water but not the propagation speed.

HESSD
9, 11267–11318, 2012

4.3 Use of remote sensing data to extract discontinuous flood surfaces

4.3.1 Acquisition and pre-processing of the MYD09A1 data

The MYD09A1 500 m, 8-day synthesis images covering the TRD (tile H22V09) from the 4 July 2002 to the 19 December 2011 were downloaded from the NASA website (434 images). In a first phase, they were processed using the LDOPE software tool (MODIS Land quality assessment group: Roy et al., 2002) to mask the pixels with a high cloud cover or aerosols. To do so, the surface reflectance state quality layer was used: pixels where aerosol quantity was low or average and the MOD35 cloud cover was clear were kept while all the others were masked. Bands 1–7 were processed, corresponding to the visual, near and mid infra-red bands. The images were then reprojected into geographical coordinates, subset to the studied area (upper left corner: 2°6′0″ S, 39°59′56.4″ E, lower right corner: 2°6′0″ S, 39°59′56.4″ E) and transformed into geotiffs using the HDF-EOS To GeoTIFF Conversion Tool (HEG v2.11, EOS, 2012). In a second phase, a geographical mask was applied to limit the study area to the Tana River floodplains. This mask was constructed manually through visual interpretation of the 90 m Shuttle Radar Topography Mission Digital Elevation Model (SRTM DEM) and only includes the TRD floodplains and surrounding areas. This mask roughly follows the Menjila-Lamu road to the north, the eastern and western terraces and the southern coastal forest and sand dunes (Fig. 1). The river mouth and the surrounding mangroves were excluded so that the regular flooding of these zones by the ocean tides was not considered.

4.3.2 NDMI threshold determination, selection of images and uncertainty estimation

To determine the threshold at which flooded and non flooded pixels were best identified, three MYD09A1 images were compared to ground truthing points acquired during extensive field trips in the TRD. A total of 1398 field points where the surrounding 500 m

HESSD
9, 11267–11318, 2012

by 500 m area was either flooded or dry were acquired during 2 flood events (May 2010 and December 2011 when respectively 254 and 211 flooded and 253 and 270 dry points were acquired) and one rainy season where no floods occurred (May 2009, with 410 dry points). The $NDWI_{Gao,M2-5}$ for each pixel was calculated as the ratio of the spectral bands 2 (B_2) and 5 (B_5): $\frac{B_2-B_5}{B_2+B_5}$. To determine the $NDWI_{Gao,M2-5}$ index threshold that best differentiated flooded and dry pixels, the percent of correctly classified image pixels was calculated at different $NDWI_{Gao,M2-5}$ values (Table 5). An upper and lower uncertainty range were also calculated to take into account the error in determining the threshold value and the cloud cover by calculating the number of non-flooded pixels wrongly classified as flooded and the number of flooded pixels wrongly classified as non flooded. The upper uncertainty range was then increased to include the clouded pixels.

5 A water-balance model of the Tana River Delta: the Tana Inundation Model (TIM)

5.1 Data constraints for hydrological modeling and applied approach

The hydrological data available (Table 2) was used to construct a unique reservoir model calibrated with the MODIS satellite imagery (Fig. 3). To do so, a four-step approach was used:

1. A sub-set of the MYD09A1 images acquired by the MODIS satellite Aqua were used to extract a discontinuous time-series of flood surfaces. In parallel, a spatial representation of the inundated zones was obtained alongside the frequency of floods corrected for cloud cover.

2. A water balance model (TIM), using simplified assumptions about the geometry of the delta and the discharge curve at the outlet, was then constructed.

HESSD
9, 11267–11318, 2012

3. The model was calibrated and validated through the GLUE methodology (Beven and Binley, 1992) by comparing it to the extracted satellite data. To do so, two cost functions are defined: the Modified Nash-Sutcliffe coefficient (MNS) and the Global Modified Nash-Sutcliffe coefficient (GMNS).

4. The temporal dynamics of inundation in the Tana River Delta throughout the past decade were obtained with an estimation of the water height, flood extent and duration, frequency and a yearly water balance were also computed. The comparison of the calculated flood frequency with the estimation of flood frequency using the MODIS imagery was a further validation of the hydrological model (Fig. 8).

5.2 Step 1: extraction of discontinuous flood surfaces, construction of a flood map and calculation of the frequency of floods using MYD09A1 images

The MODIS imagery set was used in three ways. Firstly, images presenting less than 10 % cloud cover for all seven bands (76 in total) were selected to obtain a discontinuous time-series of flooded surfaces in order to calibrate and validate the hydrological model. This set was well-distributed during the rainy and dry seasons, so that images were available during the flooded periods. For each non masked pixel within the geographical mask, the $NDWI_{Gao,M2–5}$ was calculated and the pixels with a $NDWI_{Gao,M2–5}$ value higher than the threshold value were considered as flooded. Secondly, the whole dataset of available MYD09A1 images was used to calculate the inundation frequency of each pixel for 2002–2011. The frequency of floods for each pixel was calculated as:

$$f_i = \frac{F_i}{N_T - M_i} \tag{3}$$

where f_i is the flooded frequency for pixel i, F_i the number of times the pixel was flooded, N_T the total number of images available and M_i the number of times the pixel was masked at band 2 and band 5. A map of spatial frequency of floods was then constructed.

HESSD
9, 11267–11318, 2012

Thirdly, the images were used to get a temporal frequency of flood extent using Eq. (4):

$$f_F = \frac{1}{N_T} \sum (F_{n_t} + M_t \cdot \frac{F_{n_t}}{S_T - M_t}) \quad (4)$$

where f_F is the temporal frequency of floods for the whole period, F_{n_t} and M_t respectively the total flooded and masked surface for each MODIS image t, and S_T the total studied zone. The last term represents a flood extent corrected to take into account the masked pixels. The underlying hypothesis was that the ratio of flooded extent to the visible zone was identical to the ratio of flooded extent to the clouded zone. Only images with less than 50 % cloud cover at band 2 and band 5 were used so that the former hypothesis remained plausible.

5.3 Step 2: definition of the reservoir model

5.3.1 Water balance equation

The Tana River Delta was represented as a unique reservoir. The volume, V [L^3], surface, S [L^2], and height, Z [L], of water were calculated according to Eq. (5):

$$\frac{dV}{dt} = S \cdot \frac{dZ}{dt} = Q_i + R + L - Q_s - E - I \quad (5)$$

where Q_i is the incoming discharge from the Tana River (computed after the non-linear routing model presented above, [$L^3\,T^{-1}$]), R is the rainfall over the flooded surface [$L^3\,T^{-1}$], L is the overland flow from rainfall over the sub catchment from Garsen to the estuary [$L^3\,T^{-1}$], Q_s is the outgoing discharge from the Tana River [$L^3\,T^{-1}$], E is the total evapotranspiration from the inundated area [$L^3\,T^{-1}$] and I is the total water infiltration [$L^3\,T^{-1}$].

HESSD
9, 11267–11318, 2012

5.3.2 Basic topographical settings and variable specifications

In order to obtain an ordinary differential equation (ODE), the flooded surface, outgoing discharge, infiltration and evapotranspiration were transformed as a function of the water height in the reservoir. The outflow Q_s from the reservoir, unknown in reality because of its diffuse character, was related to the height of the water stored above the reservoir's outlet at sea-level, Z_{SL}, in a classical manner, i.e.

$$Q_s = \alpha \cdot (Z - Z_{SL})^{\beta} \quad (6)$$

$Z - Z_{SL}$ represents the head loss between the reservoir and its outlet. The value of β is typically between a minimum of 0.5 for a Chezy or Manning type flow and 1.5 for a free weir flow as would rather be expected here. To express the relationship between the inundated area and the water height within the reservoir and in the absence of topographical data, a simple logistic equation was used:

$$S = \frac{K}{1 + a \cdot \exp^{-r \cdot Z}} \quad (7)$$

K represents the maximum flooded surface within the reservoir, while the parameters a and r determine the shape of the logistic curve. To reduce the number of parameters, the coefficient a was expressed as a function of the initial conditions (initial flooded surface, S_0, corresponding to the surface of permanent lakes, of 4 km^2, and the initial water height within the reservoir, Z_0) and of the two other parameters. The minimal flooded surface was constrained to 1 km^2, so that a minimal water height, Z_{min}, within the reservoir could be calculated from the parameter sets. When Z_{min} was attained, evapotranspiration and infiltration were set to nil, and the outgoing discharge equaled the sum of all incoming water so that the mass balance of the equation was preserved.

Evaporation was calculated using:

$$E = e \cdot S \quad (8)$$

HESSD
9, 11267–11318, 2012

where e is the potential evapotranspiration per surface [$\mathrm{L\,L^{-2}\,T^{-1}}$], reflecting evaporation under unrestricted availability of surface water. The potential evapotranspiration, e, was obtained from monthly estimates at Malindi from Woodhead (1968) and downscaled to an hourly timescale. Infiltration was expressed through a simple linear relationship relating it to the inundated surface, S:

$$I = c_{\mathrm{I}} \cdot S \tag{9}$$

where c_{I} is the infiltration rate per surface [$\mathrm{L\,L^{-2}\,T^{-1}}$]. Total rainfall input for the model was calculated according to the equation:

$$R = R_{\mathrm{D}} \cdot S \tag{10}$$

where R_{D} is the rainfall rate per surface [$\mathrm{L\,L^{-2}\,T^{-1}}$] and S the total area directly contributing rainfall to the floods. The surface runoff input to the model from the subcatchment was calculated as a function of the rainfall at Garissa R_{SC}:

$$L = c_{\mathrm{R}} \cdot R_{\mathrm{SC}} \cdot (S_{\mathrm{SC}} - S) \tag{11}$$

with c_{R} the runoff coefficient [$\mathrm{L\,L^{-2}\,T^{-1}}$] and S_{SC}, the size of the subcatchment after Garsen (13 700 $\mathrm{km^2}$). The rainfall data, R_{D} and R_{SC}, were respectively obtained from the TDIP and Garissa meteorological stations. R_{SC} data were mean monthly estimates downscaled to hourly estimates. The coefficients K, r, α, β, Z_{SL}, c_{I}, c_{R} and Z_0 are the topographical, flow, infiltration and overland flow parameters and initial conditions of the model that need to be calibrated (Table 3). Initial conditions were chosen at an equilibrium state, i.e. during a low flow when there was no flood event.

5.4 Step 3: calculation procedure and calibration methodology: combination of remote sensing data and hydrological modeling

The ODE was solved iteratively using the fourth-order Runge-Kutta algorithm (Atkinson, 1989) at an hourly time-step. The model was coded under R (R Development

HESSD
9, 11267–11318, 2012

Core Team, 2008) and verified by checking the closure of the water balance model for all parameter sets. Water height within the reservoir was constrained to under 10 m to keep the reservoir shape conform to the TRD.

Eight parameters needed to be defined for the TIM (Table 3). Following the equifinality concept (Beven and Binley, 1992), that states that different parameter sets for a chosen model structure can be acceptable to reproduce the observed behavior of the system, an ensemble of calibrated parameter sets was chosen through the Generalized Likelihood Uncertainty Estimation (GLUE) methodology (Beven and Binley, 1992; Beven and Freer, 2001). According to this methodology, we:

1. Defined the prior ranges of parameter values and generated random and independent sets of parameters (Table 3). All parameters were given a uniform prior distribution as no a priori information was available.

2. Defined the likelihood measure used to select the acceptable parameter sets. To do so, the most reliable measurements of the system response, the flooded surfaces obtained with the water balance model, were compared to those extracted from the MODIS satellite imagery. In analogy with the Nash-Sutcliffe efficiency, we defined our Modified Nash-Sutcliffe (MNS) efficiency likelihood function relative to flooded surfaces as:

$$\mathrm{MNS} = 1 - \frac{\sum \mathrm{RE}_i^2}{\sum (S^{\mathrm{MYD}} - \bar{S}^{\mathrm{MYD}})^2} \tag{12}$$

where RE_i (Fig. 4) is the relative error defined in Eq. (13), S^{MYD} and $\bar{S}^{\mathrm{MYD}}$ the flooded surfaces calculated at each date and the mean flooded surface from the MODIS images. As the MODIS surface data have associated uncertainties, the relative error was calculated as:

HESSD
9, 11267–11318, 2012

$$
\begin{aligned}
&S_{\min}^{\mathrm{MYD}} < S^{\mathrm{sim}} < S_{\max}^{\mathrm{MYD}}, \\
&\mathrm{RE}_1 = 0 \\
&S^{\mathrm{sim}} < S_{\min}^{\mathrm{MYD}}, \\
&\mathrm{RE}_2 = S_{\min}^{\mathrm{MYD}} - S^{\mathrm{sim}} \\
&S_{\max}^{\mathrm{MYD}} < S^{\mathrm{sim}}, \\
&\mathrm{RE}_3 = S^{\mathrm{sim}} - S_{\max}^{\mathrm{MYD}}
\end{aligned}
\tag{13}
$$

The threshold of acceptability in retaining a parameter set was defined as MNS > 0.75. Parameter sets which did not allow a full resolution of the differential equations over the entire period were discarded.

3. Ran the reservoir model with each parameter set. The time-series was separated into two periods (1 January 2002–21 September 2006 and 22 September 2006–31 December 2011). Each served for calibration and validation, through a cross-calibration approach. For each calibration period, 200 000 parameter sets were generated and those with a likelihood over 0.75 were retained. As parameter sets from both calibration periods performed satisfactorily during the validation periods, they were assembled and further restrained so that the resolution through time was complete for the whole 2002–2011 period. To further constrain the parameter sets to a more realistic ensemble, two conditions as observed in the field were further used. All parameter sets with a flooded surface lower than 150 km^2 on 31 May 2010 or higher than 10 km^2 in May 2009 were discarded. Finally, the model was ran over the entire time series.

4. Calculated the prediction limits of the model (Beven and Binley, 1992). The uncertainty range was defined by the 90th and 10th prediction quantiles obtained from the likelihood-weighted model. Indeed, because of the existence of multiple parameter sets, each parameter set gives a percentile for every time-step. In

HESSD
9, 11267–11318, 2012

doing so, all the different sets contribute to define the uncertainty range and the ensemble prediction.

The global quality of the model was assessed by calculating a modified form of the MNS (the Global Modified Nash Sutcliffe coefficient, GMNS), the Absolute Maximum Error (AME), the Mean Average Error (MAE) and the Root Mean Squared Error (RMSE), as defined by Dawson Dawson et al. (2007) (Table 4). To take into account the uncertainty of both the MODIS-derived flooded-surfaces and the uncertainty range of the water-balance model, the relative errors RE (Eq. 14 and Fig. 4) were calculated in a similar way to MNS, with $S_{0.1}^{sim}$, $S_{0.9}^{sim}$ and $\bar{S}^{MYD}$ respectively the simulated flooded surface for the 10th and 90th percentile, and the mean flooded surface calculated from the MODIS images:

$$
\begin{aligned}
&S_{0.1}^{sim} < \bar{S}^{MYD} < S_{0.9}^{sim}, \\
&RE_4 = 0 \\
&S_{0.1}^{sim} < S_{min}^{MYD} < S_{0.9}^{sim}, \\
&RE_4 = 0 \\
&S_{0.1}^{sim} < S_{max}^{MYD} < S_{0.9}^{sim}, \\
&RE_4 = 0 \\
&S_{0.9}^{sim} < S_{min}^{MYD}, \\
&RE_5 = S_{min}^{MYD} - S_{0.9}^{sim} \\
&S_{max}^{MYD} < S_{0.1}^{sim}, \\
&RE_6 = S_{0.1}^{sim} - S_{max}^{MYD}
\end{aligned}
\tag{14}
$$

This is different from the usual calculation of the quality indicators as they usually do not consider the uncertainty ranges of both the simulated and observed measurements. As we set the relative error to nil each time the respective uncertainty ranges overlap, the indicators will have a higher value. This has the advantage of taking into account the uncertainty ranges and is in accordance with the equifinality concept.

HESSD
9, 11267–11318, 2012

5.5 Step 4: extraction of hydrological processes of ecological importance

Essential variables of ecological importance for the TRD, including, flood extent, the number of flood peaks throughout 2002–2011, their mean duration, flood frequency characteristics and water height within the reservoir were calculated. Estimations of main water inputs and outputs, including river input and output discharge, overland flow, rainfall, evapotranspiration and infiltration are also provided. Finally, a mean yearly water balance was calculated for the zone.

6 Results

6.1 Remote sensing data

6.1.1 Calculation of discontinuous flooded surfaces using the MODIS imagery data

When comparing the image classification to the ground-truth data for different $NDWI_{Gao,M2–5}$ values, the percent of correctly classified pixels (92.63 %) was maximal at $NDWI_{Gao,M2–5} = 0.09$ (Table 5). For all the values of $NDWI_{Gao,M2–5}$ between 0.05 and 0.015, the percent of correctly classified pixels was always over 85 % showing that the index was not sensitive around these values. At the 0.09 threshold, 3.54 % of the non-flooded pixels were wrongly classified as flooded and 15.05 % of the flooded pixels were wrongly classified as non flooded (Table 5). The mean flooded surface was of $60 \pm 76\,km^2$ with a maximum flooded surface of $309\,km^2$.

6.1.2 Spatial extent of the inundations

The frequency at which each pixel is flooded within the Tana River Delta for 2002–2011 is mapped (Fig. 5). The total surface with a frequency $f_i > 0.01$ is of $450\,km^2$, which means that each corresponding pixel was flooded over four times in 2002–2011.

HESSD
9, 11267–11318, 2012

The highest flooded frequency is of 0.41 in the south-eastern part of the delta. This most probably corresponds to a small zone with some tidal influence. The flooded zones mainly follow the active branch of the river, the Matomba branch, then spread out within the floodplain grasslands. The areas surrounding the former active Oda branch are rarely flooded. The major lakes of the zone, the Moa, Shakababo and Bilissa Boka lakes, appear. The map corroborates well with our knowledge of the terrain. Furthermore, the former channels with riverine forests and other non flooded zones effectively appear as non flooded on the map. Lastly, all villages are out of the flooded zones, but actually close to them for easy access to pasture land, as observed in the TRD.

6.2 TIM calibration and validation

The parameters that were calibrated are presented in Table 3. During the 2002–2006 calibration period, 380 sets of parameters were selected through the GLUE methodology (Table 6). The Global Nash-Sutcliffe efficiency coefficient, GMNS, was of 0.93 and 0.87 for the calibration and validation periods. During the 2006–2011 calibration period, 116 sets of parameters were selected (Table 6). The GMNS was respectively of 0.84 and 0.89 for the calibration and validation periods. The model seems better adapted to the 2002–2006 period, with more parameter sets and higher GMNS values compared to 2006–2011.

As the parameter sets from both calibrations are equifinal, i.e. they respond to the same selective criteria and are all acceptable parameters sets for the proposed model, they were combined to form an ensemble of parameters used in the next steps. After further restriction, 150 parameter sets were finally retained. The global model performance for each period and the whole 2002–2011 period are summarized in Table 6. GMNS, AME and MAE were respectively 0.92, 137 km^2 and 9 km^2 for the entire period. In the light of these criteria, the proposed model performs well.

The parameters do not present any structure within the prior distribution space. However, Z_0 and Z_m are highly correlated (0.82), r and α show a correlation of 0.63, α and β a correlation of 0.43, c_1 and α a correlation of −0.53. The correlation between the

HESSD
9, 11267–11318, 2012

other parameters are all under 0.33 (and mostly under 0.1). The correlation of Z_0 and Z_m can be explained by the fact that the starting dates of the model were chosen when the system was at equilibrium, i.e. at its minimal value when water height within the reservoir is identical to the water height at the outlet.

6.3 Hydrological processes of ecological importance in the Tana River Delta

6.3.1 Temporal dynamics of inundation throughout the past decade

The flooded surfaces simulated by TIM for 2002–2011 are represented in Fig. 6. The periodicity of the floods is well reproduced, with the flooding seasons corresponding to the rainy seasons. Most of the data points as calculated using the MODIS images fall within the 10th and 90th percentiles of the hydrological model, except for the second flooding season of 2007. According to the hydrological model, the maximum flood peak of the past decade occurred in December 2002, with a medium and 90th percentile value of respectively 397 and 564 km^2. On the contrary, the long rainy seasons flood events of 2011 seem to have been negligible, with a flooded surface inferior to 100 km^2. This has been confirmed through field observations. The model has an uncertainty range linked to the lack of essential data such as a Digital Elevation Model and the scarcity of recent discharge measurements at the delta inlet. For example, the maximum 10th and 90th percentiles flood extent for the 2002 flood event are 279 km^2 and 564 km^2. Remaining clouds also contributes to the uncertainty of the model. Indeed, the measured flood extent with the MODIS imagery for the long rainy season of 2009 is close to nil as indeed observed in the field but the clouds cover nearly 100 km^2, drastically increasing the upper uncertainty range. Finally, because of the chosen likelihood function, the relative uncertainty for low inundation extents is larger than for the high values. The model should therefore better capture large flooded areas.

The simulated water height within the reservoir for 2002 to 2011 was computed. The maximum calculated water height within the reservoir for the 90th percentile is of 2.1 m with a mean median water height throughout the whole period of 1.4 m. According to

HESSD
9, 11267–11318, 2012

expert and local knowledge, the mean water height over the grassy floodplains of the Tana River Delta has not exceeded 2 m in the last decade which is in agreement with this model. Once again, the uncertainty linked to the water height calculation is high and interpretation of the water heights must be done with precaution. However, this model gives an approximate range of water height values, and maybe more interestingly, an idea of the rate of change and difference between the minimum and maximum water height during a flood event.

Inflow discharge, rainfall, overland flow, output discharge, evapotranspiration and infiltration were calculated (Fig. 7). Except for the input discharge, the latter all have corresponding uncertainty ranges. Maximum 90th percentile modeled rain, overland flow, evapotranspiration, infiltration and river inflow and outflow were respectively of $1.9 \times 10^6\,m^3\,h^{-1}$, $9.8 \times 10^4\,m^3\,h^{-1}$, $1.5 \times 10^5\,m^3\,h^{-1}$, $5.2 \times 10^5\,m^3\,h^{-1}$, $7.0 \times 10^5\,m^3\,h^{-1}$ and $7.3 \times 10^5\,m^3\,h^{-1}$ for a flooded surface of $564\,km^2$.

6.3.2 Flood extent and duration

According to the hydrological model, 16 flood events with flood peaks over $100\,km^2$ (median value) occurred during the 2002–2011 studied period (Table 7). Their mean duration was 41 days. Out of these 16 floods, five lasted less than 15 days. These events seem quite regular, with at least one flood per year of over $100\,km^2$ during more than 15 days. However, because of the calibration procedure of TIM, small flooded surfaces could be over-estimated. Flood events of a bigger scale seem rare, with a median number of flood events over $200\,km^2$ of only 5 for the 18 recorded potential flooding periods. These floods would only occur on average every 2 yr, even though there are two flooding seasons per year. Their mean median and 90th percentile duration were of 18 ± 7 days and 17 ± 13 days, with the longest 90th percentile flood duration of 44 and 42 days in May 2002 and November 2004. Finally, according to the model, flood events over $300\,km^2$ only occurred 0 to 6 times (in 2002, 2003, 2004 and 2006) and were of short duration.

HESSD
9, 11267–11318, 2012

6.3.3 Flood frequency characteristics

The observed frequency of flooded days at different inundation extents for 2002–2011 were compared between TIM and the MODIS results (Fig. 8). The trend between the two different curves is identical with a decrease in the frequency of high floods. The flooded frequency for floods between 0 and 10 km^2 is respectively of 0.46 and 0.44 for the MODIS images and for the median values of TIM. Both seem to capture an interesting feature of the inundation pattern. Indeed, flood frequency is high for relatively small flooded surfaces then decreases rapidly for surfaces inferior to 50 km^2. The frequency then reaches a plateau for flooded surfaces between 50 km^2 and 200 km^2. The latter seems to be the normal flood extent range for the observed discharges. According to the model, the median cumulated observed frequencies of floods over 100 km^2 and 200 km^2 are of 0.10 and 0.02, meaning that this state occurs 10 % and 2 % of the time.

6.3.4 A water balance for the Tana River Delta

A water balance for each selected parameter set was computed. The mean total volume of water transiting through the system was of 28.6 ± 0.2 km^3, corresponding to a yearly inflow of 3.28 km^3. A mean absolute difference of 0.14 % between the incoming and outgoing flows for all parameter sets was observed and attributed to the use of numerical resolution and its related approximations. The difference is considered negligible.

The model allows to compute a system water balance (Table 8) using the median values of the parameter ensemble. The total modeled median yearly inflow and outflow are of respectively 3.16 km^3 and 2.88 km^3. It appears that the river inflow corresponds to over 96 % of the total water inflow during the analyzed period and the river outflow to over 89 % of the total water outflow. It confirms that the river discharge coming from Garissa and therefore the upper catchment is the major process controlling the flooding events within the Tana River Delta.

HESSD
9, 11267–11318, 2012

7 Discussion

The propagation characteristics (discharge-discharge and time delay relationships) of floods within the lower stretch of the Tana River have been described. Despite a lack of knowledge of the Garissa-Garsen 250 km^2 stretch, the river discharge at Garsen has been reconstituted for the 1963–2011 period from discontinuous discharge measurements at Garissa.

The methodology applied, a combination of hydrological modeling and remote-sensing techniques, has proven to be efficient in describing the hydrological system in a ground data scarce and high cloud-cover context. The MYD09A1 product can be used in clouded or non-clouded areas where medium temporal and spatial resolutions are required. They can be an alternative or complementary data source to radar imagery to measure flood extent in ungauged floodplains as the frequent overpass of the Aqua and Terra satellites makes them a good candidate to monitor rapidly changing inundation areas. The methodology to extract the flooded surfaces could be used with alternative satellite images.

The simple water-balance approach adopted here was relevant to study the TRD system where information on the internal properties and processes was limited. TIM enhances our understanding of the hydrology of the Lower Tana River by providing a temporal and spatial range for the floods of the Tana River in its deltaic floodplains. In a next step, the spatial characteristics of the floods could be better defined by incorporating multiple reservoir units. Indeed, a visual inspection of the derived MOD09A1 flood surface images showed that the spatial distribution of the floods was not constant throughout a flood event: the delta is first flooded in its upper part before the flood propagates into the more southern floodplains.

Before any model improvement of the TRD hydrological system can be expected, a better knowledge of the system itself is necessary. In the current situation, the lack of data is the main limiting factor. Firstly, regular discharge or water height measurements at the inlet, outlet and other strategic locations (channel bifurcations, etc.)

HESSD
9, 11267–11318, 2012

should be privileged. Secondly, a precise topographic map would help describe the volume-surface-water height relationships and hence the channel-overland flow dynamics. Lastly, a regular monitoring of the floods through the acquisition and analysis of high-resolution satellite imagery, in combination with ground truthing data, should be undertaken. Without these, a more precise understanding of the inundation dynamics and the development of a more sophisticated model seem challenging.

TIM is a tool that can be used to study the impact of the modifications of the hydrological regime. Despite the associated uncertainty, the model outputs are suitable to undertake preliminary analyses of the ecological responses of the wetland system following hydrological changes or upstream development. For model simulations, precautions should be taken when extrapolating it to higher discharges or other time-periods. Indeed, the model has not been validated for extreme flood events such as those that occurred in 1997–1998. In this case, other important factors such as rainfall in the middle catchment, which are only partly accounted for in the model, may play a role. The Tana River has also undergone major changes in the past with the construction of hydro-electric reservoirs that could have modified the geomorphology and other characteristics of the TRD. The temporal and spatial resolution requirements for the simulation should therefore be carefully pondered. All in all, after taking some basic precautions, the results presented here can be used to study the ecological responses to past hydrological changes or future water-use scenarios. This would be a major step in assessing the changing properties and functions of the Tana River wetlands or the impact of new dam constructions on the provided ecosystem services and could improve the management strategies of the natural resources of the Tana River Delta.

8 Conclusions

In this study, the hydrological dynamics of the ungauged floodplains of the Tana River Delta were modeled in the context of scarce data. The major hydrological processes were determined and a temporal and spatial representation of the floods

HESSD
9, 11267–11318, 2012

provided alongside a yearly water-balance estimate. The simple water-balance approach adopted here has proven to be a pertinent approach when studying this system where information on its internal properties and processes are limited. The methodology, a combination of hydrological modeling and flood-mapping using the MODIS products, should be applicable to other areas where data is scarce and a medium spatial resolution required. The results presented here can be used to study past and future hydrological changes for a better management of the Tana River Delta.

Acknowledgements. This project was financed by the French Ministry of Environment in the framework of the project "Eaux et Territoires", by the Research Institute for Development (IRD) and by the LISAH laboratory. We thank the Water Resource Management Authority for providing the discharge data, the Kenya Department of Meteorology and the Tana Delta Irrigation Project for the rainfall data. The National Museums of Kenya (NMK), the People, Livestock and the Environment (PEL) research group at the International Livestock Research Institute (ILRI) in Nairobi and the IRD representation in Eastern Kenya are also acknowledged.

References

Alsdorf, D. E., Rodriguez, E., and Lettenmaier, D. P.: Measuring surface water from space, Rev. Geophys., 45, RG2002, doi:10.1029/2006RG000197, 2007. 11272

Atkinson, K. E.: An Introduction to Numerical Analysis, John Wiley & Sons, New York, ISBN 978-0-471-50023-0, 1989. 11285

Bader, J., Lamagat, J., and Guiguen, N.: Management of the Manantali Dam on the Senegal River: quantitative analysis of a conflict of objectives, Hydrolog. Sci. J., 48, 525–538, doi:10.1623/hysj.48.4.525.51415, 2003. 11269

Barbier, E. and Thompson, J.: The value of water: floodplain versus large-scale irrigation benefits in Northern Nigeria, Ambio, 27, 434–440, 1998. 11269

Bauer, P., Gumbricht, T., and Kinzelbach, W.: A regional coupled surface water/groundwater model of the Okavango Delta, Botswana, Water Resour. Res., 42, W04403, doi:10.1029/2005WR004234, 2006. 11271

HESSD

9, 11267–11318, 2012

Belaud, G., Cassan, L., Bader, J., Bercher, N., and Feret, T.: Calibration of a Propagation Model in Large River Using Satellite Altimetry, in: 6th International Symposium on Environmental Hydraulics, 23–25 June, Athens, 2010. 11278

Beven, K. and Binley, A.: The future of distributed models – model calibration and uncertainty prediction, Hydrol. Process., 6, 279–298, doi:10.1002/hyp.3360060305, 1992. 11270, 11282, 11286, 11287

Beven, K. and Freer, J.: Equifinality, data assimilation, and uncertainty estimation in mechanistic modelling of complex environmental systems using the GLUE methodology, J. Hydrol., 249, 11–29, doi:10.1016/S0022-1694(01)00421-8, 2001. 11286

Daily, G.: Nature's Services: Societal Dependence on Natural Ecosystems, Island Press, Washington, DC, 1997. 11269

Dawson, C. W., Abrahart, R. J., and See, L. M.: HydroTest: a web-based toolbox of evaluation metrics for the standardised assessment of hydrological forecasts, Environ. Modell. Softw., 22, 1034–1052, doi:10.1016/j.envsoft.2006.06.008, 2007. 11278, 11288, 11306

Duvail, S. and Hamerlynck, O.: Mitigation of negative ecological and socio-economic impacts of the Diama dam on the Senegal River Delta wetland (Mauritania), using a model based decision support system, Hydrol. Earth Syst. Sci., 7, 133–146, doi:10.5194/hess-7-133-2003, 2003. 11269

Duvail, S. and Hamerlynck, O.: The Rufiji River flood: plague or blessing?, Int. J. Biometeorol., 52, 33–42, 2007. 11269

Duvail, S., Médard, C., Hamerlynck, O., and Nyingi, D. W.: Land and water grabbing in an East African coastal wetland: the case of the Tana Delta, Water Alternat., 5, 322–343, 2012. 11274, 11275

Emerton, L.: Tana River, Kenya: Integrating Downstream Values Into Hydropower Planning, Case Studies in Wetland Valuation 6, in: Integrating wetland economic values into river basin management, edited by: IUCN, International Union for the Conservation of Nature, available at: http://cmsdata.iucn.org/downloads/casestudy06tana.pdf (last access: October 2012), 2003. 11274

EOS: HDF-EOS To GeoTIFF Conversion Tool (HEG), available at: http://newsroom.gsfc.nasa.gov/sdptoolkit/HEG/HEGHome.html, last access: October 2012. 11280

Fekete, B. F. and Vörösmarty, C. J.: The current status of global river discharge monitoring and potential new technologies complementing traditional discharge measurements, in:

HESSD
9, 11267–11318, 2012

Proceedings of the PUB Kick-off meeting held in Brasilia, 20–22 November 2002, vol. 309, IAHS Publ., 129–136, 2007. 11270
Feng, L., Hu, C., Chen, X., Cai, X., Tian, L., and Gan, W.: Assessment of inundation changes of Poyang Lake using MODIS observations between 2000 and 2010, Remote Sens. Environ., 121, 80–92, 2012. 11272
Gao, B.: NDWI – a normalized difference water index for remote sensing of vegetation liquid water from space, Remote Sens. Environ., 58, 257–266, doi:10.1016/S0034-4257(96)00067-3, 1996. 11273, 11313
Hamerlynck, O., Luke, Q., Nyange, T., Duvail, S., and Leauthaud, C.: Range Extension, Imminent Threats and Conservation Options for Two Endangered Primates: the Tana River Red Colobus Procolobus rufomitratus rufomitratus (Peters, 1879) and the Tana River Mangabey Cercocebus galeritus (Peters, 1879) in the Lower Tana Floodplain and Delta, Kenya, African Primates, in press, 2012. 11274
Hughes, D. A., Andersson, L., Wilk, J., and Savenije, H. H. G.: Regional calibration of the Pitman model for the Okavango River, J. Hydrol., 331, 30–42, doi:10.1016/j.jhydrol.2006.04.047, 2006. 11271
International Livestock Research Institute: available at: http://192.156.137.110/gis/ (last access: 1 October 2012), 2012. 11273, 11275
Islam, A. S., Bala, S. K., and Haque, M. A.: Flood inundation map of Bangladesh using MODIS time-series images, J. Flood Risk Manage., 3, 210–222, doi:10.1111/j.1753-318X.2010.01074.x, 2010. 11272
Kenya: Vegetation and present land-use map – Garsen, 8101:50000. Series Y731A, sheet 179/3 Edition 1-JICA, Tech. rep., Kenya Soil Survey, Japan, 1984a. 11276
Kenya: Vegetation and present land-use map – Witu, 8121:50000. Series Y731A, sheet 179/4 Edition 1-JICA, Tech. rep., Kenya Soil Survey, Japan, 1984b.
Lamagat, J. P., Morel-Seytoux, J., and Albergel, J.: Analyse de la propagation des ondes de crue, Hydrol. Continent., 8, 113–137, 1993. 11278
Lamagat, J. P., Sambou, S., and Albergel, J.: Analyse statisique de l'ecoulement d'un fleuve dans une plaine d'inondation: application aux cotes maximales du fleuve Niger dans le cuvette lacustre, in: L'hydrologie tropicale: geoscience et outil pour le developpement: melanges a la memoire de Jean Rodier, IAHS Press, Wallingford, UK, p. 238, 1996. 11269
Leauthaud, C.: Diagnostic agraire dans le delta du Tana, au Kenya, Master's thesis, AgroParisTech, Paris, France, 2009. 11274

HESSD
9, 11267–11318, 2012

Leauthaud, C., Duvail, S., Hamerlynck, O., Paul, J.-L., Cochet, H., Nyunja, J., Albergel, J., and Grünberger, O.: Floods and livelihoods: impact of changing water resources on wetland agro-ecological production systems in the Tana River Delta, Kenya, Global Environ. Chang., in review, 2012. 11274

Leblanc, M., Lemoalle, J., Bader, J. C., Tweed, S., and Mofor, L.: Thermal remote sensing of water under flooded vegetation: new observations of inundation patterns for the "small" Lake Chad, J. Hydrol., 404, 87–98, doi:10.1016/j.jhydrol.2011.04.023, 2011. 11272

Loth, P. (Ed.): The Return of the Water: Restoring the Waza Logone Floodplain in Cameroon, IUCN, Gland, Switzerland and Cambridge, UK, xvi + 156, 2004. 11269

Mahe, G., Orange, D., Mariko, A., and Bricquet, J. P.: Estimation of the flooded area of the inner delta of the River Niger in Mali by hydrological balance and satellite data, in: Hydro-Climatology: Variability and Change, edited by: Franks, S., Boegh, E., Blyth, E., Hannah, D., and Yilmaz, K., vol. 344 of IAHS Publication, 25th General Assembly of the International Union of Geodesy and Geophysics, Melbourne, Australia, June 28–July 7, 2011, 138–143, 2011. 11271

Maingi, J. and Marsh, S.: Quantifying hydrologic impacts following dam construction along the Tana River, Kenya, J. Arid Environ., 50, 53–79, doi:10.1006/jare.2000.0860, 2002. 11269, 11274

McFeeters, S.: The use of the normalized difference water index (NDWI) in the delineation of open water features, Int. J. Remote Sens., 17, 1425–1432, 1996. 11273

Merritt, D. M., Scott, M. L., Poff, N. L., Auble, G. T., and Lytle, D. A.: Theory, methods and tools for determining environmental flows for riparian vegetation: riparian vegetation-flow response guilds, Freshwater Biol., 55, 206–225, doi:10.1111/j.1365-2427.2009.02206.x, 2010. 11269, 11270

Millennium Ecosystem Assessment: Ecosystems and Human Well-being: Wetlands and Water Synthesis, Tech. rep., World Resources Institute, Washington, DC, 2005. 11269

Milzow, C., Kgotlhang, L., Bauer-Gottwein, P., Meier, P., and Kinzelbach, W.: Regional review: the hydrology of the Okavango Delta, Botswana – processes, data and modelling, Hydrogeol. J., 17, 1297–1328, doi:10.1007/s10040-009-0436-0, 2009. 11269, 11271

Milzow, C., Krogh, P. E., and Bauer-Gottwein, P.: Combining satellite radar altimetry, SAR surface soil moisture and GRACE total storage changes for hydrological model calibration in a large poorly gauged catchment, Hydrol. Earth Syst. Sci., 15, 1729–1743, doi:10.5194/hess-15-1729-2011, 2011. 11271

HESSD
9, 11267–11318, 2012

Mitsch, W. J. and Gosselink, J.: Wetlands, Wiley, New York, 2000. 11269
Oliesak, A.: Suivi par télédétection de la dynamique de crue du delta intérieur du Niger pour l'élaboration d'un modèle de fonctionnement hydraulique, Master's thesis, Université Paris Diderot, Paris, France, 2008. 11273
Ordoyne, C. and Friedl, M. A.: Using MODIS data to characterize seasonal inundation patterns in the Florida Everglades, Remote Sens. Environ., 112, 4107–4119, doi:10.1016/j.rse.2007.08.027, 2008. 11272
Poff, N. L. and Zimmerman, J. K. H.: Ecological responses to altered flow regimes: a literature review to inform the science and management of environmental flows, Freshwater Biol., 55, 194–205, doi:10.1111/j.1365-2427.2009.02272.x, 2010. 11270
Prigent, C., Matthews, E., Aires, F., and Rossow, W.: Remote sensing of global wetland dynamics with multiple satellite data sets, Geophys. Res. Lett., 28, 4631–4634, doi:10.1029/2001GL013263, 2001. 11268
Prigent, C., Papa, F., Aires, F., Jimenez, C., Rossow, W. B., and Matthews, E.: Changes in land surface water dynamics since the 1990s and relation to population pressure, Geophys. Res. Lett., 39, L08403, doi:10.1029/2012GL051276, 2012. 11269
R Development Core Team: R: a language and environment for statistical computing, R Foundation for Statistical Computing, Vienna, Austria, ISBN 3-900051-07-0, availabe at: http://www.r-project.org (last access: 1 October 2012), 2008. 11286
Republic of Kenya: Kenya Population and Housing Census, Tech. rep., Central Bureau of Statistics, available at: https://opendata.go.ke/Population/Census-Volume-1-Question-1-Population-Households-a/wd27-eki2 (last access: 1 October 2012), 2010.
Rogers, A. and Kearney, M.: Reducing signature variability in unmixing coastal marsh thematic mapper scenes using spectral indices, Int. J. Remote Sens., 25, 2317–2335, doi:10.1080/01431160310001618103, 2004. 11273
Roy, D., Borak, J., Devadiga, S., Wolfe, R., Zheng, M., and Descloitres, J.: The MODIS land product quality assessment approach, Remote Sens. Environ., 83, 62–76, 2002. 11280
Sakamoto, T., Van Nguyen, N., Kotera, A., Ohno, H., Ishitsuka, N., and Yokozawa, M.: Detecting temporal changes in the extent of annual flooding within the Cambodia and the Vietnamese Mekong Delta from MODIS time-series imagery, Remote Sens. Environ., 109, 295–313, doi:10.1016/j.rse.2007.01.011, 2007. 11272

HESSD
9, 11267–11318, 2012

Sippel, S., Hamilton, S., Melack, J., and Novo, E.: Passive microwave observations of inundation area and the area/stage relation in the Amazon River floodplain, Int. J. Remote Sens., 19, 3055–3074, doi:10.1080/014311698214181, 1998. 11272

Sivapalan, M., Takeuchi, K., Franks, S., Gupta, V., Karambiri, H., Lakshmi, V., Liang, X., McDonnell, J., Mendiondo, E., O'Connell, P., Oki, T., Pomeroy, J., Schertzer, D., Uhlenbrook, S., and Zehe, E.: IAHS decade on Predictions in Ungauged Basins (PUB), 2003–2012: shaping an exciting future for the hydrological sciences, Hydrolog. Sci. J., 48, 857–880, doi:10.1623/hysj.48.6.857.51421, 2003. 11270

Teferi, E., Uhlenbrook, S., Bewket, W., Wenninger, J., and Simane, B.: The use of remote sensing to quantify wetland loss in the Choke Mountain range, Upper Blue Nile basin, Ethiopia, Hydrol. Earth Syst. Sci., 14, 2415–2428, doi:10.5194/hess-14-2415-2010, 2010. 11269

Terer, T., Stevenson, G., and Gichuki, N.: Socio-economic values and traditional strategies of managing wetland resources in Lower Tana River, Kenya, Hydrobiologia, 527, 3–14, 2004. 11274

Ticehurst, C. J., Dyce, P., and Guerschman, J. P.: Using passive microwave and optical remote sensing to monitor flood inundation in support of hydrologic modelling, in: 18th World IMACS Congress and MODSIM09 International Congress on Modelling and Simulation: Interfacing Modelling and Simulation With Mathematical and Computational Sciences, edited by: Anderssen, R., Braddock, R., and Newham, L., Australia, combined IMACS World Congress/Modelling and Simulation Society-of-Australia-and-New-Zealand (MSSANZ)/18th Biennial Conference on Modelling and Simulation, Cairns, Australia, 13–17 July 2009, 3747–3753, 2009. 11272

Tockner, K. and Stanford, J.: Riverine flood plains: present state and future trends, Environ. Conserv., 29, 308–330, doi:10.1017/S037689290200022X, 2002. 11269

Toogood, S. E., Joyce, C. B., and Waite, S.: Response of floodplain grassland plant communities to altered water regimes, Plant Ecol., 197, 285–298, doi:10.1007/s11258-007-9378-6, 2008. 11269

United Nations Development Programme: Kenya National Human Development Report 830 2009. Youth and Human Development: Tapping the Untapped Resource, Tech. rep., United Nations Development Programme, Nairobi, Kenya, 2010. 11274

Vitousek, P., Mooney, H., Lubchenco, J., and Melillo, J.: Human domination of Earth's ecosystems, Science, 277, 494–499, doi:10.1126/science.277.5325.494, 1997. 11268

HESSD
9, 11267–11318, 2012

Wolski, P., Savenije, H. H. G., Murray-Hudson, M., and Gumbricht, T.: Modelling of the flooding in the Okavango Delta, Botswana, using a hybrid reservoir-GIS model, J. Hydrol., 331, 58–72, doi:10.1016/j.jhydrol.2006.04.040, 2006. 11271

Woodhead, T.: Studies of potential evaporation in Kenya, Tech. rep., Water development department, Ministry of Natural Resources, Republic of Kenya, 1968. 11285

Xu, H.: Modification of normalised difference water index (NDWI) to enhance open water features in remotely sensed imagery, Int. J. Remote Sens., 27, 3025–3033, 2006. 11273

Zahar, Y., Ghorbel, A., and Albergel, J.: Impacts of large dams on downstream flow conditions of rivers: aggradation and reduction of the Medjerda channel capacity downstream of the Sidi Salem dam (Tunisia), J. Hydrol., 351, 318–330, doi:10.1016/j.jhydrol.2007.12.019, 2008. 11269

Zeilhofer, P. and Schessl, M.: Relationship between vegetation and environmental conditions in the Northern Pantanal of Mato Grosso, Brazil, J. Biogeogr., 27, 159–168, doi:10.1046/j.1365-2699.2000.00357.x, 2000. 11269

HESSD
9, 11267–11318, 2012

Table 1. Mean water flow per season (equivalent to half a hydrological year) at each station and the resulting water volume ratio between the stations. The number of seasons (Nb) used and the periods considered for each calculation are specified.

	Mean and sd	Nb	Period
Water flow per season at Garissa (km^3)	2.51 ± 1.34	115	1941–2009
Water flow per season at Garsen (km^3)	1.56 ± 0.46	23	1951–1992
Volume ratio	0.76 ± 0.28	22	1951–1992

HESSD
9, 11267–11318, 2012

Table 2. Hydrological, climate and remote sensing data used in this study.

Data	Dates	Use
Discharge at Garissa	1941–2009	Preanalysis/Flood routing model
Discharge at Garsen	1951–1998	Preanalysis/Flood routing model
Discharge at Garissa	2002–2011	TIM
MYD09A1 (76 images)	2002–2011	TIM (calibration/validation)
MYD09A1 (434 images)	2002–2011	TIM (flood extent map, flood frequency)
Rainfall at Garissa	2002–2011	TIM
Rainfall at Garsen	2002–2011	TIM
Potential evapotranspiration	2002–2011	TIM

HESSD
9, 11267–11318, 2012

Table 3. Definition of TIM model parameters. a and Z_{min} were calculated from the calibrated parameters.

Parameter	Signification	Range/Value	Unit	Calibrated
α	parameter for discharge at outlet	$0–10 \times 10^9$	–	Yes
β	parameter for discharge at outlet	0.2–1.7	–	Yes
K	maximum flooded surface	300–700	km^2	Yes
a	parameter for logistic equation	–	–	No
r	parameter for logistic equation	0–40	–	Yes
c_R	overland runoff coefficient	0–0.05	–	Yes
c_I	infiltration rate	0–25	$mm\,day^{-1}$	Yes
Z_0	initial water height	0–2	m	Yes
Z_{SL}	water level at outlet	0–5	m	Yes
Z_{min}	minimal water level	–	m	No
S_0	initial flooded surface	4	km^2	No
S_{min}	minimal flooded surface	1	km^2	No
S_{SC}	subcatchment surface	13 700	km^2	No

HESSD
9, 11267–11318, 2012

Table 4. Quality indicators of the models, as defined by Dawson et al. (2007). For the flood routing model, the relative errors (RE) are defined using the observed and simulated discharges. MNS and GMNS are defined in the text.

Quality indicators	Abbreviation	Equation
Absolute Mean Error	AME	$\max \lvert \mathrm{RE} \rvert$
Mean Absolute Error	MAE	$\frac{1}{n} \sum \lvert \mathrm{RE} \rvert$
Root Mean Square Error	RMSE	$\sqrt{\frac{1}{n} \sum \mathrm{RE}^2}$

HESSD
9, 11267–11318, 2012

Table 5. Number of correctly classified MODIS pixels compared to the field ground truth data at different $NDWI_{Gao,M2-5}$ threshold values. Classification was divided into either flooded or dry points. Percent over or under-estimation of flooded surfaces were calculated as the ratio of the total number of incorrectly classified pixels per status (dry or flooded) on the total number of points per status.

Date of ground truth data	Status	Nb	th = 0.05	th = 0.06	th = 0.07	th = 0.08	th = 0.09	th = 0.10	th = 0.11	th = 0.12
25 May 2009	dry	410	407	409	409	410	410	410	410	410
25 May 2010	dry	270	167	186	213	230	244	255	261	264
19 December 2011	dry	253	196	226	238	245	246	248	249	251
% over-estimation		933	17.47	12.00	7.82	5.14	3.54	2.14	1.39	0.86
25 May 2010	flooded	211	195	191	185	183	181	175	170	163
19 December 2011	flooded	254	238	233	230	224	214	207	196	179
% under-estimation		465	6.88	8.82	10.75	12.47	15.05	17.85	21.29	26.45
Total (%)		1398	86.05	89.06	91.20	92.42	92.63	92.63	91.99	90.63

Total (%): total percent of correctly classified pixels, th: threshold, Nb: Total number points.

HESSD
9, 11267–11318, 2012

Table 6. Cost functions for the calibration and validation periods and the whole 2002–2011 period (Aggregate).

Set	Number of parameter sets	Calibration/ Validation	Period	AME (km^2)	MAE (km^2)	RMSE (km^2)	GMNS
Calibration 1	380	Calibration	2002–2006	82.36	7.71	17.08	0.93
	380	Validation	2006–2011	122.65	15.95	31.63	0.87
Calibration 2	116	Calibration	2006–2011	125.64	19.37	34.25	0.84
	116	Validation	2002–2006	103.38	9.77	21.98	0.89
Aggregate	150		2002–2011	137.77	9.29	24.22	0.90

HESSD
9, 11267–11318, 2012

Table 7. Number of floods and their mean duration for 2002–2011. 10th percentile/median/90th percentile.

Flood extent	Total number of floods	Mean duration and sd (days)
over 100 km^2	15/16/22	26 ± 21/41 ± 24/40 ± 30
over 200 km^2	7/5/18	10 ± 3/18 ± 7/17 ± 13
over 300 km^2	0/5/6	0/3 ± 2/9 ± 5

HESSD
9, 11267–11318, 2012

Table 8. Annual water balance for 2002–2011 (median values of TIM).

	Input (km^3)		Output (km^3)
Inflow	3.16	Outflow	2.88
Rain	0.04	Evapotranspiration	0.11
Overland flow	0.10	Infiltration	0.24
Total	3.30	Total	3.23

HESSD
9, 11267–11318, 2012

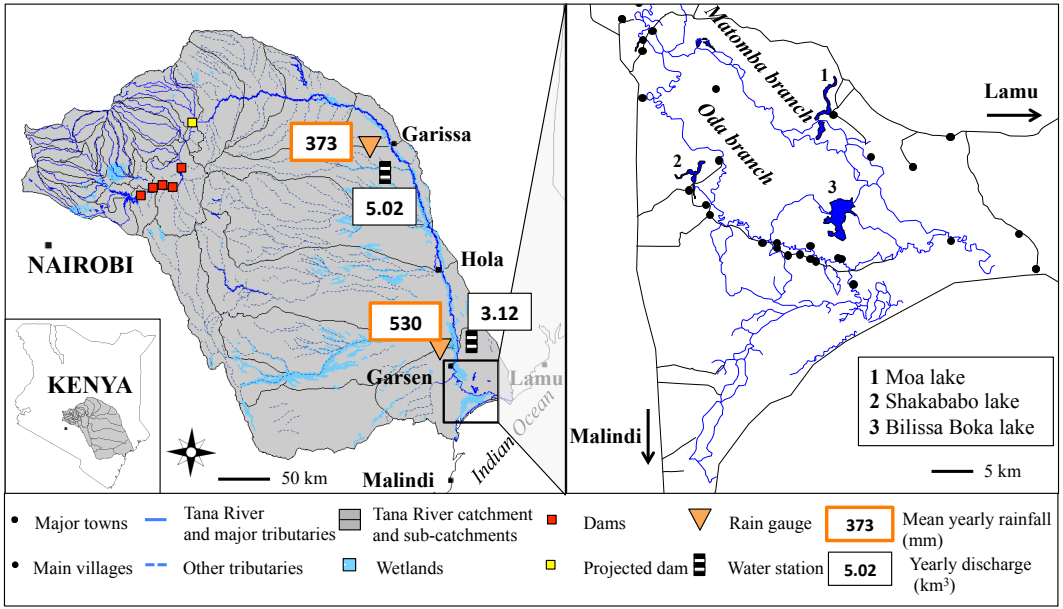

Fig. 1. Left: the Tana River, its catchment, sub-catchments and main hydrological characteristics. The location of the precipitation and discharge data used for this study are specified. Right: the Tana River Delta, its two major channels, lakes, villages and roads.

HESSD
9, 11267–11318, 2012

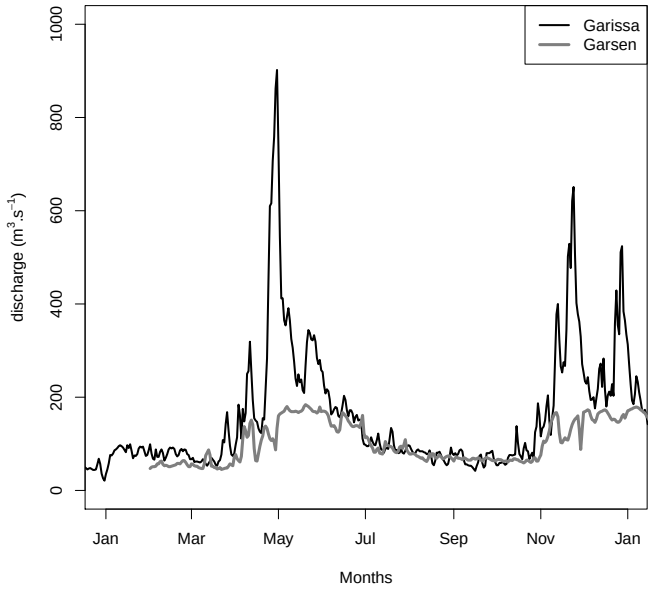

Fig. 2. Discharge data for the Garissa, Q_1, and Garsen, Q_2, stations in 1988

HESSD
9, 11267–11318, 2012

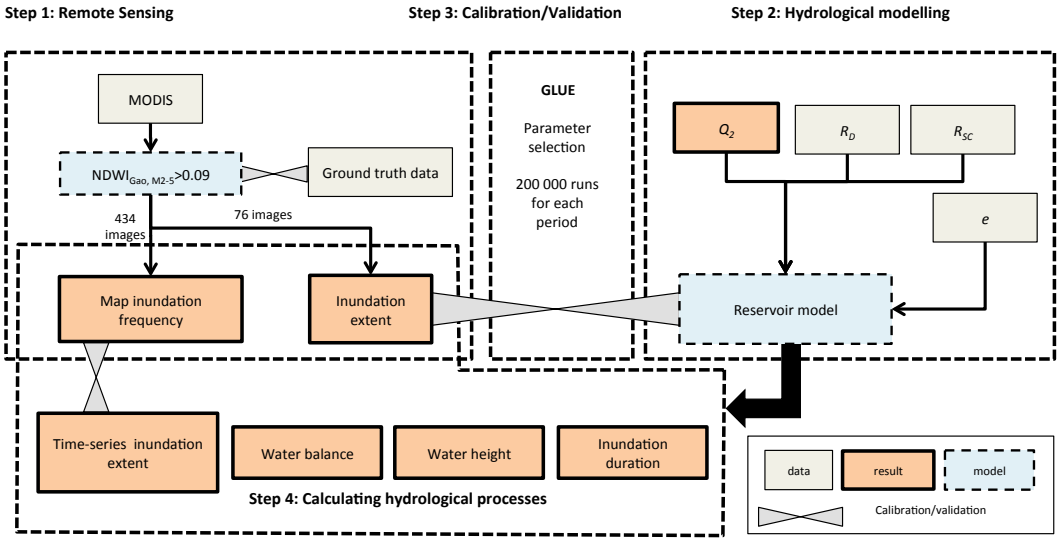

Fig. 3. Workflow diagram identifying the models, their input variables, the calibration/validation processes and the main results of the study. Q_2: discharge at Garsen, R_D: rainfall within the delta, R_{SC}: rainfall at Garissa, $NDWI_{Gao,M2-5}$: Normalized Difference Water Index of Gao (1996).

HESSD
9, 11267–11318, 2012

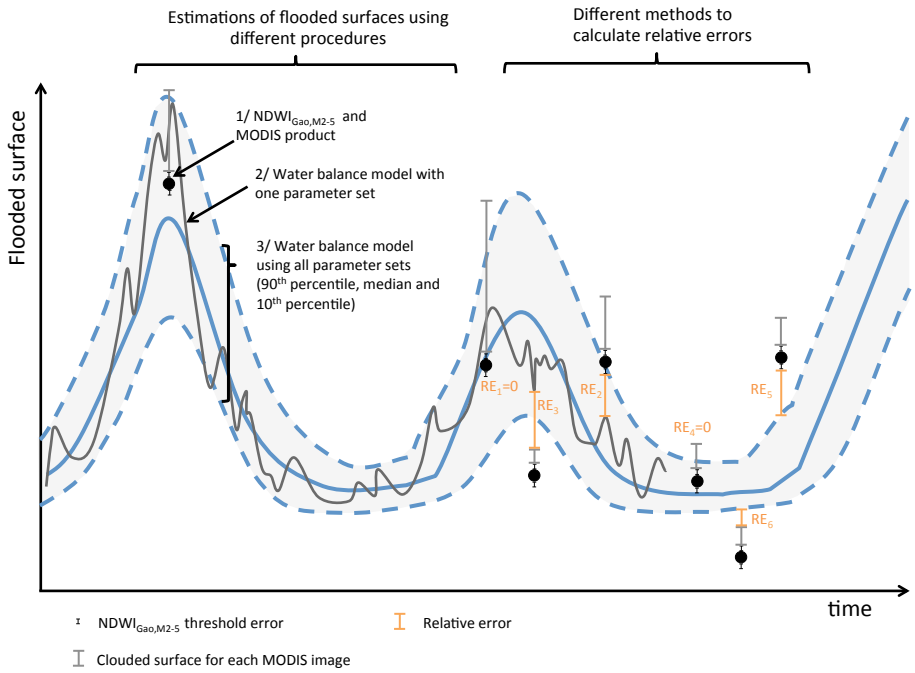

Fig. 4. Simplified scheme depicting the flooded surfaces and other essential definitions. Left: flooded surfaces and uncertainty range obtained from (1) MODIS imagery, (2) the water balance model with one parameter set and (3) the water balance model using all the parameter sets. In the latter, the dotted curves represent the 90th and 10th percentile and the full curve the median flooded surface when using all the parameter sets. Right: representation of the different relative errors.

HESSD
9, 11267–11318, 2012

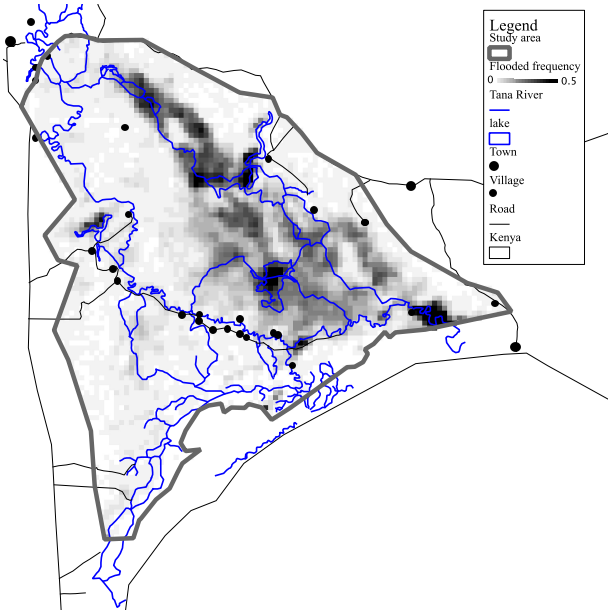

Fig. 5. Map of the frequency of flooding, extracted from MODIS images (2002–2011).

HESSD
9, 11267–11318, 2012

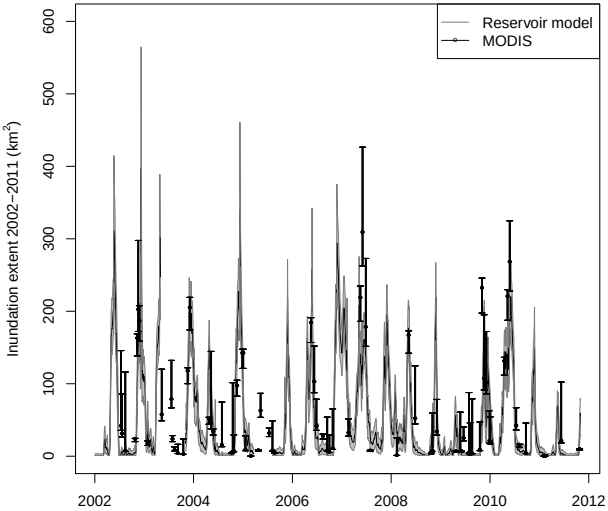

Fig. 6. Flooded surface in the delta, 2002–2011, as computed by TIM or extracted from the MOD09A1 imagery.

HESSD
9, 11267–11318, 2012

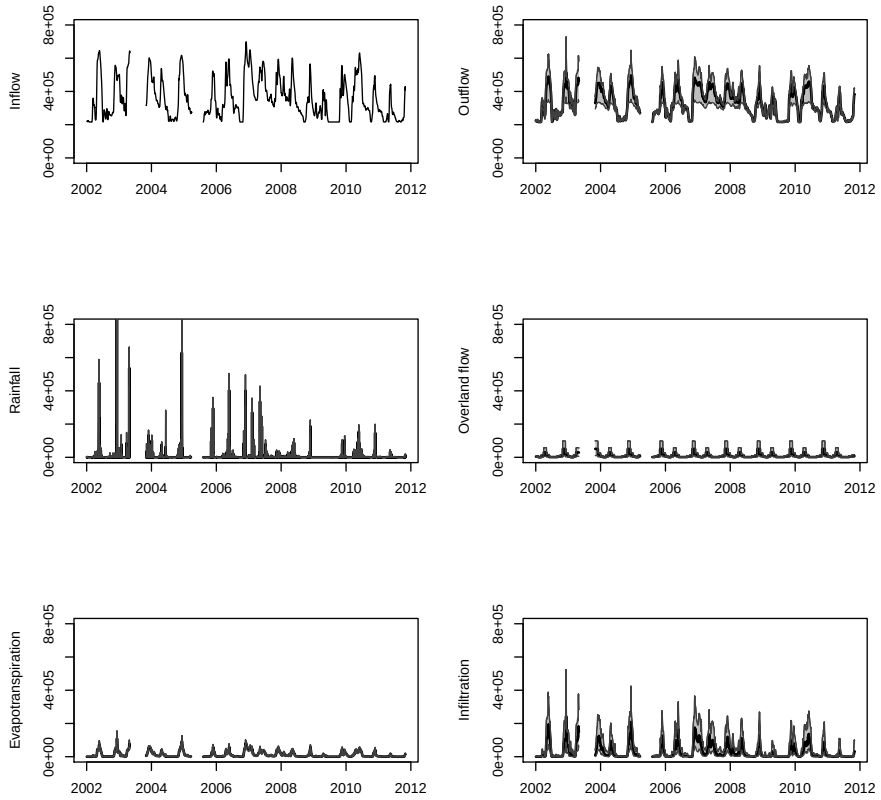

Fig. 7. Simulated hourly inflow, outflow, rainfall, overland flow, evapotranspiration and infiltration for 2002–2011 as computed by TIM. The grey envelope represents the lower 10th and upper 90th percentile estimations.

HESSD
9, 11267–11318, 2012

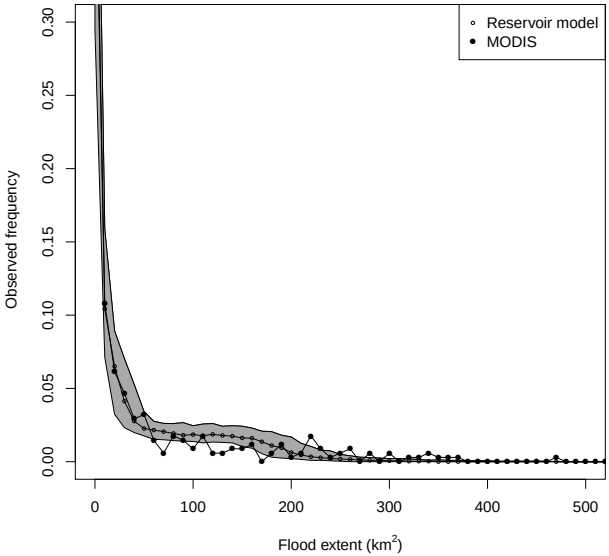

Fig. 8. Frequency of flooded days as a function of flooded surface for the MODIS imagery and the hydrological model. The median value and the 10th–90th percentiles are depicted for TIM.

HESSD
9, 11267–11318, 2012